

X-ray-photoelectron-diffraction study of InAs/InP(001) heterostructures

E. Bergignat, M. Gendry, and G. Hollinger

*Laboratoire d'Electronique, Automatismes et Mesures Electriques, Ecole Centrale de Lyon,
36 avenue Guy de Collongue, F-69131, Ecully Cedex, France*

G. Grenet

*Centre de NanoAnalyse et Technologie de Surface, Université Claude Bernard, Lyon I,
43 boulevard du 11 Novembre 1918, F-69622, Villeurbanne Cedex, France*

(Received 22 November 1993)

The growth mode and the strain of InAs thin films grown on InP(001) were measured by x-ray-photoelectron diffraction (XPD). Since the effects of a (2×4) reconstruction at the InAs film surface may drastically overlap those of the growth mode, we also investigated a (2×4) reconstructed GaAs(001) surface as a standard for this kind of reconstruction. It appears that this type of reconstruction does not induce significant effects on the polar angular distributions recorded within the (110) and the $(\bar{1}\bar{1}0)$ planes. XPD measurements showed that the formation of thin InAs films on InP(001) by As stabilization is better described by a multilayer model of the InAs/InAs_xP_(1-x)/InP type than by a layer-by-layer InAs/InP model. For the strained 10-Å-thick InAs film grown on InP(001), the best agreement found between experiment and theory gives a vertical lattice expansion of 7.5%. This value is between 6.1%, the expansion obtained from the macroscopic linear elasticity theory, and 9.5%, the expansion obtained when assuming that the atomic bond length is retained.

I. INTRODUCTION

Highly strained mismatched heteroepitaxial systems are of increasing importance from a fundamental point of view due to their unique electronic properties and to their potential applications in microelectronics and optoelectronics. However, a high density of defects can be generated when thick epitaxial layers are grown on highly mismatched substrates. At present, high-quality strained layers can only be obtained for thicknesses not exceeding a critical value above which structural defects such as three-dimensional (3D) islands or dislocations appear. Therefore there is great interest in understanding the growth processes and in characterizing the structural properties of heterojunctions on the atomic scale.

Various techniques may be used to characterize the structural properties of surface and thin-film heterostructures. Techniques such as low-energy electron diffraction, reflection high-energy electron diffraction (RHEED), and scanning tunneling microscopy are essentially sensitive to the top layers. In contrast, x-ray diffraction is bulk sensitive with an analysis depth of a few hundred to a thousand angstroms below the surface. Between these two extremes, grazing-incidence x-ray diffraction (GIXRD), x-ray photoelectron diffraction (XPD), and to some extent transmission electron microscopy (TEM) probe the top few tens of angstroms below the surface. The element specificity in XPD makes this technique particularly well suited to investigating the atomic arrangement at surfaces and interfaces in the first steps of heteroepitaxial growth. In fact, this technique is now known to be sensitive to surface reconstruction, adsorbate geometries, surface disorder, surface segregation, and strain in epitaxial layers.¹⁻¹¹

In this work, we have used the XPD technique to describe the structural properties of InAs thin films grown on InP(001) either by As stabilization or by molecular-beam epitaxy (MBE), the bulk samples InAs(001) and InP(001) being taken as references. However, we have to bear in mind that InAs(001) thin films may present the same surface reconstructions as GaAs(001), and that the occurrence of such surface reconstructions may interfere with the study of the growth mode and/or the quantification of the strain. We therefore first investigated GaAs(001) bulk samples, which exhibit well-known surface reconstructions.

This paper is divided into four parts. The first one is the introduction, the second deals entirely with the experimental apparatus and sample preparations. The third contains the experimental and theoretical results as well as the related discussion. The last part summarizes all the concluding remarks.

II. EXPERIMENT

A. Experimental apparatus

The experimental apparatus consisted of a Vacuum Science Workshop (VSW) surface-analysis chamber connected to a Riber 2300 MBE reactor, via a horizontal transfer chamber. The surface reconstructions, morphology, and orientation of the *in situ*-grown samples were monitored by RHEED.

The focused unpolarized monochromatic Al $K\alpha$ ($h\nu = 1486.6$ eV) x-ray source and the analyzer were in the same plane. The x-ray source was at a fixed angle of 50° relative to the photoelectron-detector direction. Polar plots were obtained by rotating the sample around the projection of the incident beam direction in the plane

of the sample surface, while azimuthal plots were achieved by rotation around the normal to the sample. The polar angles were measured with respect to the sample normal. The high-precision angular manipulator allowed polar and azimuthal sample rotation with precision better than 1° . The acceptance angle of the spectrometer was about 2° .

B. Sample preparation

All the samples were mounted on a molybdenum holder using indium solder. The sample temperature was monitored by a thermocouple and an infrared pyrometer previously calibrated using the melting point (525°C) of InSb. Two sets of structures were studied: (i) bulk samples InAs(001), InP(001), and GaAs(001) used as references and (ii) thin InAs films obtained either by As stabilization or by MBE growth.

1. InAs(001) bulk sample

The InAs substrate was a (001)-oriented undoped *n*-type wafer, of "standard quality," from Sumitomo. The InAs(001) surfaces were prepared as either As stabilized or MBE grown.

(a) *As-stabilized InAs(001)*. Following deoxidation with a HF-ethanol solution, residual surface contamination was removed during thermal treatment at 500°C under 10^{-5} Torr As pressure. Only (1×1) bulk streaks were observed in the RHEED pattern during the As treatment. This As treatment was followed by ultrahigh-vacuum annealing at 400°C for 20 min in order to eliminate residual chemisorbed As atoms.

(b) *MBE-grown InAs(001)*. A $2\text{-}\mu\text{m}$ epitaxial layer was grown by MBE at 450°C , with an As-to-In beam equivalent pressure (BEP) ratio of 100. A (2×4) RHEED pattern was observed during growth. The growth was ended by simultaneously closing the In and As shutters and decreasing the temperature to 300°C under 10^{-9} Torr As pressure before transferring the sample

into vacuum. This latter procedure was used in order to limit the number of residual chemisorbed As atoms.

2. InP(001) bulk sample

The InP substrate was a (001)-oriented undoped *n*-type wafer, of "epi-ready quality," from Sumitomo. The InP surface was deoxidized by HF-ethanol treatment and then annealed under vacuum at 350°C for 20 min to remove surface contamination. The final RHEED pattern exhibited only (1×1) bulk streaks.

3. GaAs(001) bulk sample

The GaAs substrate was a (001)-oriented undoped *n*-type wafer, of "epi-ready quality," from Wacker. The MBE experimental procedure was almost the same as for InAs but the growth temperature was 600°C and the As-to-Ga BEP ratio was 17. The final GaAs(001) surface was annealed up to 400°C to remove residual chemisorbed As.

4. InAs/InP(001) thin films

The lattice-parameter mismatch between InAs and InP is 3.2%. The critical thicknesses for the 2D-3D growth-mode onset and for plastic relaxation through dislocations are of the order of 10 and 20 Å, respectively.¹² The InAs/InP heterojunctions were obtained either by As stabilization or by MBE growth.

(a) *As stabilized InP(001)*. As-stabilized InP surfaces were prepared by thermally annealing InP(001) surfaces first cleaned with HF-ethanol, under 10^{-5} Torr As overpressure. Three As-stabilized InP(001) surfaces were prepared at three different temperatures which correspond to three types of RHEED patterns: (1) annealing at 450°C which corresponds to a (2×1) RHEED pattern; (2) annealing at 550°C , the point where the twofold periodicity disappears in the RHEED pattern, indicating the existence of a rough surface; and (3) annealing for a

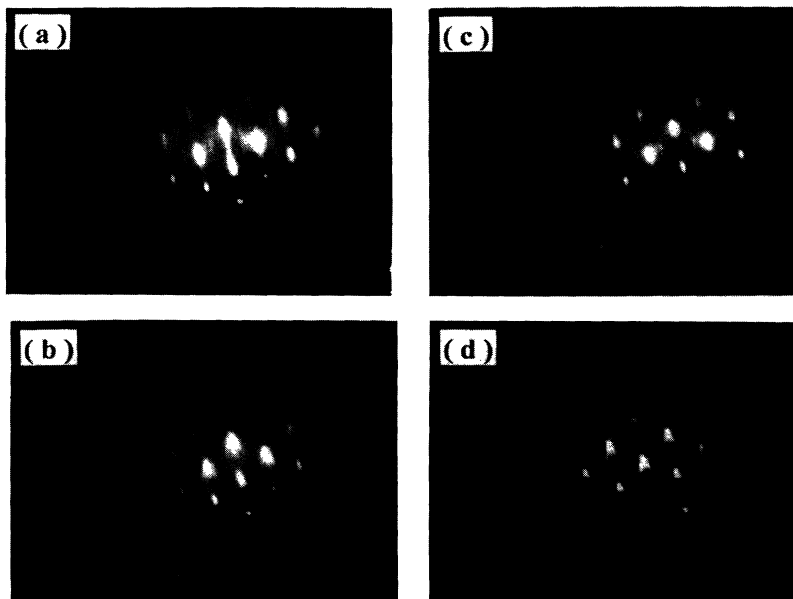


FIG. 1. RHEED patterns for (a) a $10\text{-}\text{\AA}$ -thick InAs film grown on InP(001) along the $[110]$ direction, (b) a $10\text{-}\text{\AA}$ -thick InAs film grown on InP(001) along the $[1\bar{1}0]$ direction, (c) a $36\text{-}\text{\AA}$ -thick InAs film grown on InP(001) along the $[110]$ direction, and (d) a $36\text{-}\text{\AA}$ -thick InAs film grown on InP(001) along the $[1\bar{1}0]$ direction. The V-shaped spots indicate a (114) faceting.

nuclear directions for the zinc-blende bulk structure within the low-index planes (001), (110), and (1 $\bar{1}$ 0). These crystallographic data are summarized in Table I in units of the lattice constant, i.e., 5.6532 Å for GaAs, 6.0584 Å for InAs, and 5.8687 Å for InP.¹⁵

Along the [001] direction, the zinc-blende structure consists of planes containing only group-III elements (Ga,In) alternating with planes containing only group-V elements (As,P). In the following discussion, one group-III element layer or one group-V element layer will be referred to as "one atomic monolayer" (1 ML). The relative positions of the group-III atoms with respect to the group-V atoms in a (110) plane are the same as those of the group-V atoms with respect to the group-III atoms in a (1 $\bar{1}$ 0) plane. In other words, the group-III element sublattice is transformed into the group-V element sublattice by performing a 90° rotation around the [001] axis. It should also be noted that, as far as the surface is concerned, there are two types of (110) and (1 $\bar{1}$ 0) planes, depending on whether or not (type 1 or type 2) they contain the atoms belonging to the top layer (see Fig. 2). This means that, if the top layer is reconstructed, only one out of two of the (110) or (1 $\bar{1}$ 0) planes is affected. Therefore, just in view of these geometrical considerations, the effects induced by a top-layer reconstruction may be thought to be particularly weak for the polar angular distributions (PAD's) recorded within these two (110) and (1 $\bar{1}$ 0) planes. In fact, this is the reason for the initial choice of these PAD's, since we are mainly concerned with the study of pseudomorphic InAs/InP(001) heterojunction and not with that of the reconstruction.

The calculations in this paper were performed using the single-scattering-cluster (SSC) method¹⁰ which gives good results when simulating the PAD's obtained with high-kinetic-energy photoelectrons. The initial-state

wave function emerging from the emitting atom is assumed to be well described by a spherical wave function: the photoionization asymmetrical effects are negligible, because in our experimental apparatus the light is unpolarized. This spherical wave traveling away is approximated by plane waves when it reaches a scattering atom. The scattering amplitudes and phase shifts were estimated from standard atomic tabulations.¹⁶ Indeed, it has been shown¹ that the curved-wave correction¹⁷ is rather small at high kinetic energy even for very small distances. Five layers of emitting atoms were included. Such a slab is thick enough to allow numerical convergence to be reached. The top layer is always assumed to be made up of group-V elements and thus these five layers correspond to a probed depth of $2a$ for the group-V elements and to a probed depth of $2.25a$ for the group-III elements, a being the lattice constant. The whole cluster contains at least 500 atoms, which are either emitters or scatterers. Inelastic attenuation is taken into account via the classical mean free path fixed at $5a \sim 30$ Å.

To allow an easy comparison between theoretical and experimental results, each calculated polar curve $I(\theta)$ was normalized by the slowly varying part of the polar scan, $P(\theta)$, called "background," to give $I_n(\theta)$ through the relationship

$$I_n(\theta) = P(\theta)I(\theta) + P(\theta).$$

The experimental polar plots recorded along different azimuths and/or for different compounds were normalized in such a way that their intensities are equal to 100% at normal emission. In doing this, the effects of the photoemission cross sections are completely eliminated and attention can be paid exclusively to fine structures. All the figures are reported in this paper using the same scale to allow direct comparison.

TABLE I. Characteristics of internuclear axes for the group-III element and the group-V element as emitters within the (110) and (1 $\bar{1}$ 0) planes for an ideal bulk crystal. "Layer" means the relative position of the scatterer layer above the emitter layer (in units of the lattice parameter), θ is the angle of the internuclear axis relative to the surface (in degrees), and "Length" means the emitter-scatterer distance (in units of the lattice parameter).

Scatterer	Layer	(110) plane		Scatterer	Layer	(1 $\bar{1}$ 0) plane	
		θ	Length			θ	Length
Group-V emitter							
III	0.25	54.7	0.43	III	0.75	25.2	0.82
V	1.00	0.0	1.00	V	1.00	0.0	1.00
III	0.25	76.7	1.09	V	1.00	35.3	1.22
V	1.00	35.3	1.22	III	0.75	54.7	1.30
III	1.25	15.8	1.30	V	1.00	54.7	1.73
III	1.25	40.3	1.64	III	1.75	11.4	1.79
V	1.00	54.7	1.73	III	0.75	67.0	1.92
Group-III emitter							
V	0.75	25.2	0.82	V	0.25	54.7	0.43
III	1.00	0.0	1.00	III	1.00	0.0	1.00
III	1.00	35.3	1.22	V	0.25	76.7	1.09
V	0.75	54.7	1.30	III	1.00	35.3	1.22
III	1.00	54.7	1.73	V	1.25	15.8	1.30
V	1.75	11.4	1.79	V	1.25	40.3	1.64
V	0.75	67.0	1.92	III	1.00	54.7	1.73

A. InAs(001) and InP(001) bulk samples as references

Figure 3 shows the experimental and theoretical PAD's for the In 4*d* (1467.1 eV) and As 3*d* (1425.5 eV) core levels within the (110) plane and the (1 $\bar{1}$ 0) plane for a MBE-grown InAs(001) sample. As expected from the above geometrical considerations, the As 3*d* (In 4*d*) PAD in the (110) plane is similar to the In 4*d* (As 3*d*) PAD in the (1 $\bar{1}$ 0) plane. Obviously, when a comparison is made with the internuclear directions (Table I), there exists a simple relationship between the maxima and the positions (indicated by arrows) of the first neighbors of the emitting atoms. The peaks that originate from pure forward scattering occur for relatively short interatomic emitter-scatterer spacings, whereas for large emitter-scatterer distances, the forward-focusing effects compete with interference effects. As an example, for the As 3*d* emission in the (110) plane, the peaks labeled (a) and (d) at 0° and 55°, respectively, clearly have a pure forward-scattering character since they can be directly related to the nearest scatterers. Their positions correspond exactly to internuclear axes in the experimental curves as well as in the theoretical calculations. In contrast, the peaks labeled (b) and (c) do not have their ideal internuclear directions, i.e., 16° and 35° in the experimental curve: the first one has shifted to a higher angle θ by about 5° and the second one seems to be split. The same trends may be observed in the (1 $\bar{1}$ 0) plane for the In 4*d* emission. Turning now to the In 4*d* emission in the (110) plane [or to the As 3*d* emission in the (1 $\bar{1}$ 0) plane], the peaks labeled (a) and (f) are unambiguously of a forward-focusing character whereas peaks like (b) and (e) have a more complex ori-

gin. The experimental intensities are more or less well reproduced by the simulation except for peaks (d) and (f), which are underestimated. To check the effects of the photoelectron kinetic energy on the shape of PAD's, we have simultaneously recorded, for an As-stabilized InAs(001) sample, the In 4*d* (1467.1 eV), In 3*d* (1042.1 eV), As 3*d* (1425.4 eV), and As 2*p* (164.0 eV) core levels within the (110) plane. The experimental results and corresponding SSC calculations are reported in Fig. 4: The In 3*d* and In 4*d* PAD's are quite similar (in spite of their different mean free paths), whereas the As 2*p* and As 3*d* PAD's are completely different. Neither the positions nor the intensities of the As 2*p* XPD peaks are well taken into account by the SSC calculations. This is because the focusing effect decreases as the effects neglected in the SSC model, such as multiple-scattering and backscattering processes, increase.

In Fig. 5, the In 3*d* (1042.1 eV), In 4*d* (1467.1 eV), and P 2*p* (1357.1 eV) PAD's for InP(001) are reported for the (110) plane. These PAD's were measured to characterize the substrate on which the InAs epitaxial growth was made. Although P atoms are relatively light ($Z=15$) compared to As ($Z=33$), here again the reported polar curves are more characteristic of the site of the photoelectron-emitter atoms than of the atomic species of the emitter and/or of the scatterer.

B. GaAs (001) as reference for the (2×4) reconstruction

Since XPD probes the top few tens of angstroms below the surface, the XPD features may be sensitive to top-layer reconstruction. Though the InP(001) surface is

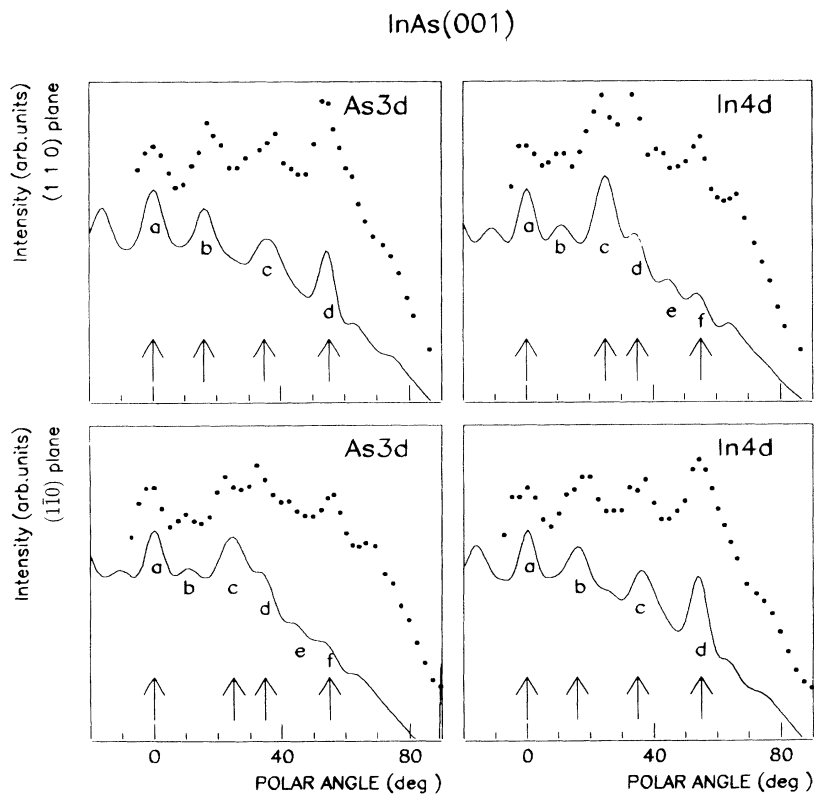


FIG. 3. Experimental (dots) and calculated (plain lines) polar plots for the As 3*d* and the In 4*d* core levels in the (110) and (1 $\bar{1}$ 0) planes for a MBE-grown InAs(001) sample.

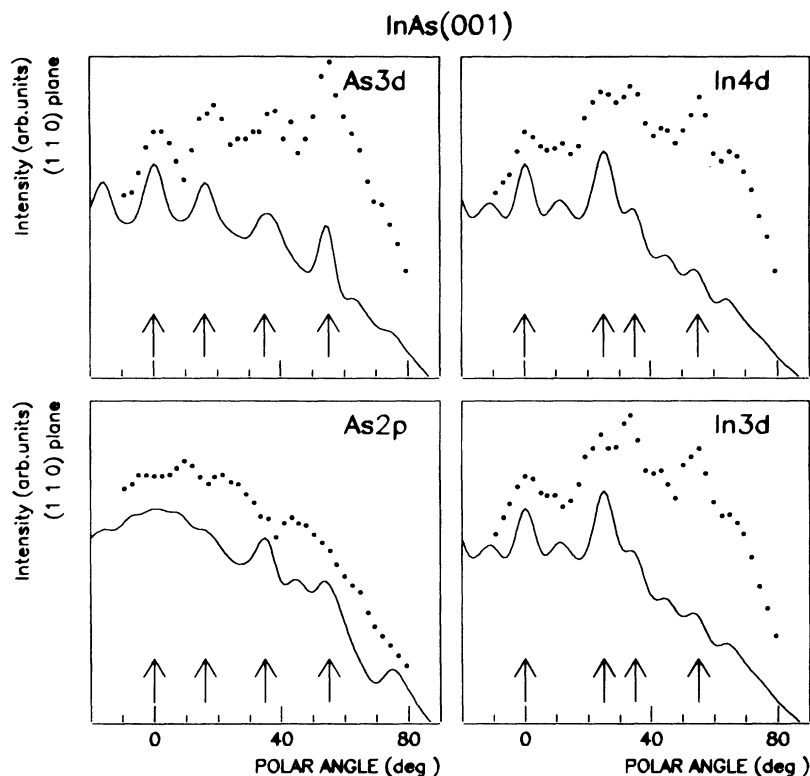


FIG. 4. Experimental (dots) and calculated (plain lines) polar plots for the As $3d$, the As $2p$, the In $4d$, and the In $3d$ core levels in the (110) plane for an As-stabilized InAs(001) sample.

thought to be unreconstructed, this is not the case for the InAs(001) surface which may present the same surface reconstruction as GaAs(001). This point is of crucial importance because we are interested in bulk properties rather than in surface ones: any strong effects arising from surface reconstructions may merge with the bulk

effects due to the growth mode or strain we are looking for. We carried out some studies on GaAs(001), whose surface reconstructions are better known than those of InAs(001) and thus may be regarded as a standard.

Depending on the cooling procedure after growth (sample temperature, arsenic pressure, etc.), the

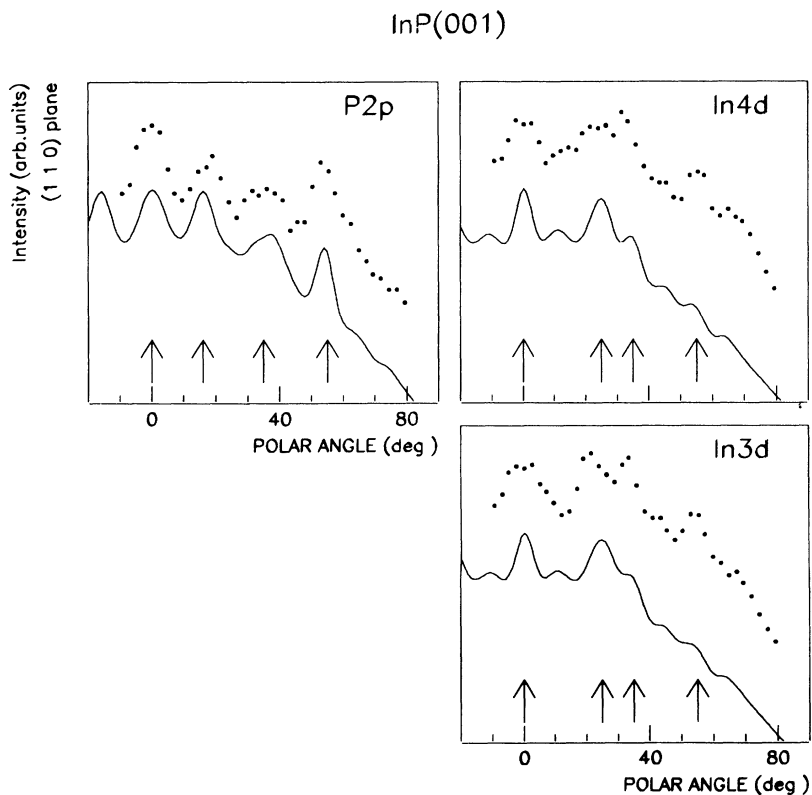


FIG. 5. Experimental (dots) and calculated (plain lines) polar plots for the P $2p$, In $4d$, and the In $3d$ core levels in the (110) plane for an InP(001) sample.

GaAs(001) surfaces can exhibit different surface reconstructions corresponding to different [As]/[Ga] surface concentrations.¹⁸⁻²⁴ They range from the As-rich (2×4) reconstruction which corresponds to $\sim 75\%$ of 1 ML of arsenic in the top layer, to the Ga-rich (4×2) reconstruction, which corresponds to $\sim 25\%$ of 1 ML of arsenic in the top layer. It has been shown that these reconstructions arise in both cases from the formation of surface As-As or Ga-Ga dimers in the $[1\bar{1}0]$ direction. According to the calculations of Qian, Martin, and Chadi,²¹ the As dimers for the (2×4) reconstruction shift slightly up by $0.019a$ along the $[001]$ direction, and each As atom within a dimer is pushed from its ideal position in an unreconstructed surface by $\pm 0.126a$ along the $[1\bar{1}0]$ direction. Note that, when the surface is cooled under As pressure, a (4×4) surface reconstruction may be observed due to the absorption of 1 ML of As on an As-rich surface. In this case, the As dimers lie along the $[110]$ direction.

Figure 6 shows the As $3d$ and the Ga $3d$ PAD's measured within the (110) and the $(1\bar{1}0)$ planes for a MBE-grown GaAs(001) surface with a (2×4) surface reconstruction. The Ga $3d$ and the As $3d$ photoelectrons have very close kinetic energies (1468 and 1425 eV) and their atomic numbers (31 and 33) are close. Therefore, any observed difference between the curves from emitters in the same crystallographic sites can be imputed to chemical and/or structural effects at the surface, and in particular to surface reconstruction. As may be seen in Fig. 6, no significant differences can be found between the PAD's corresponding to emitters in the same crystallographic

site. This absence of effects due to (2×4) reconstruction in the experimental PAD's within the (110) and $(1\bar{1}0)$ planes is in agreement with SSC simulations. Theoretical curves calculated for an unreconstructed surface (plain line), an As-full-coverage (2×1) reconstructed surface (dashed line), and an As-full-coverage (4×4) reconstructed surface (dotted line) are compared in Fig. 6 with the experimental results. The theoretical (2×1) surface can be used to investigate the properties of a (2×4) surface since it contains more As dimers than the latter: 100% instead of 75%. These calculations confirm that the (2×1) reconstruction [and consequently the (2×4) reconstruction] induces only slight effects in the (110) plane and almost no effects in the $(1\bar{1}0)$ plane. For the (4×4) reconstruction, the situation is reversed: the reconstruction effects are more obvious in the (110) plane than in the $(1\bar{1}0)$ plane. Thus, even if a (2×4) reconstruction is present at the InAs thin-film surfaces, its effects within the (110) and the $(1\bar{1}0)$ planes are completely dominated by the contributions of the bulk layers. Finally, let us compare the InAs and the GaAs PAD's (Figs. 3 and 6). Similar features at the same angles clearly demonstrate that, for high-kinetic-energy photoelectrons, the crystallographic properties are the dominant factor and that variations in scattering amplitudes do not induce important differences in the XPD maxima positions and intensities. However, when comparing Fig. 3 (or 4) with Fig. 6, we see that the PAD's do not drop to zero in the same way. We relate this quite different background behavior to differences in surface preparation (especially temperature). In fact, the GaAs sample

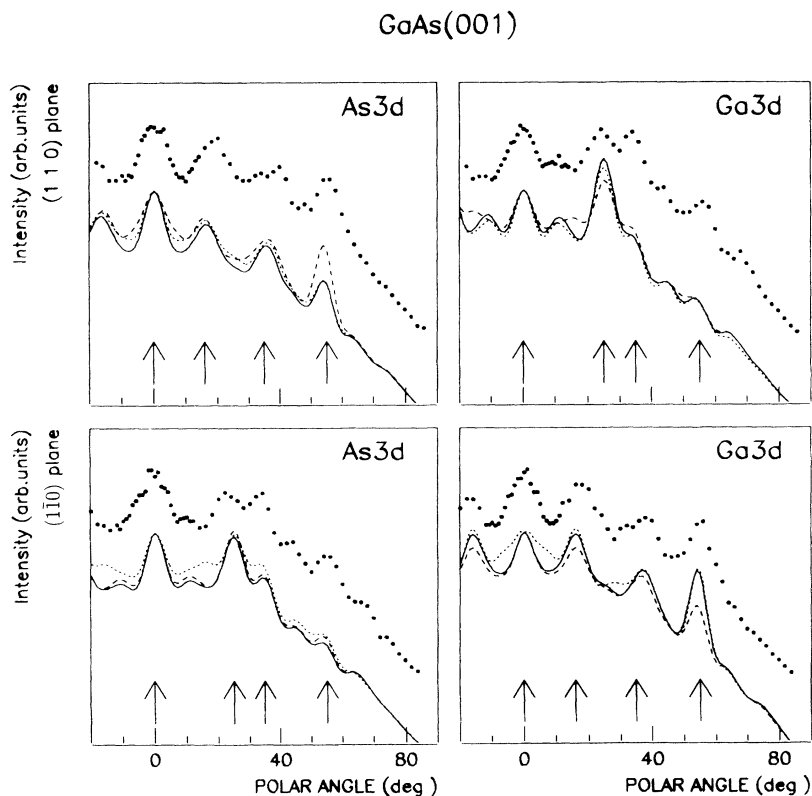


FIG. 6. Experimental (dots) and calculated polar plots for the As $3d$ and the Ga $3d$ core levels in the (110) and $(1\bar{1}0)$ planes for a MBE-grown GaAs(001) sample. Calculations without any reconstruction are indicated by plain lines while calculations taking into account a full-As-coverage (2×1) reconstruction and a full-As-coverage (4×4) reconstruction are noted by dashed lines and by dotted lines, respectively.

(which was annealed up to 400°C under vacuum) has less chemisorbed As randomly distributed on the surface crystallographic sites than the InAs sample (which was not annealed and for which growth was carried out at a lower temperature). In the InAs case, the local order is preserved (and thus the positions of the XPD maxima are not affected) but the slowly varying part of the PAD's reflects the excess of As on the surface. This abnormal background in InAs PAD's may be associated with the long-range order of the surface. This assumption will be confirmed in the next section when looking at background evolution during InAs growth on InP.

C. The growth of InAs/InP(001) heterostructures by As stabilization of InP(001) surfaces

Pseudomorphic InAs/InP surface quantum wells can be formed as a result of As-P exchange when InP wafers are heated under arsenic overpressure above the InP congruent-evaporation temperature. XPS measurements¹³ have indicated the formation of 1–3 equivalent bilayers (1 BL equals 1 ML of In plus 1 ML of As) of InAs on InP when the annealing temperature ranges from 450°C to 575°C. However, the InAs/InP interface is not chemically abrupt. Our purpose in this section is to take advantage of a comparison between experimental and theoretical XPD results to evaluate quantitatively the penetration of the As atoms into the crystal. For this purpose, we simulated InAs growth within a layer-by-layer model. The resulting As 3d PAD's are reported in Fig. 7. No strain effect or background were introduced in the simulation. We performed calculations for both the

In-rich surfaces with 100% In atoms in the surface layer (dashed lines) and the As-rich surfaces with 100% As atoms in the surface layer (plain lines), even though the former is not experimentally obtainable. As may be seen from Fig. 7, the theoretical XPD curves for the In-rich and As-rich surfaces are too close to each other to allow the proportion of As atoms within the top layer to be evaluated. However, this quantification may be deduced from interpretation of the RHEED patterns: for example, a (2×4) reconstruction corresponds to 75% of 1 ML of As. In Fig. 7, we see typical XPD maxima successively appearing in As 3d PAD's when the As atoms replace P atoms in a layer. In the (110) plane, the first four curves a–d, corresponding to the sequence [In,As, substrate] with 1 ML of As, [As,In,As, substrate] with 2 ML of As, [In,As,In,As, substrate] with 2 ML of As again, and [As,In,As,In,As, substrate] with 3 ML of As, show only one peak at 55° and a more complex structure at a grazing angle (around 80°). The bulk aspect is reached with the next sequence [In,As,In,As,In,As, substrate] with 3 ML of As (curve e). Quite different behavior is found for the As 3d emission in the (1 $\bar{1}$ 0) plane: no diffraction peak appears for the first two sequences [In,As, substrate] with 1 ML of As, and [As,In,As, substrate] with 2 ML of As (curves a and b); diffraction peaks appear only with the third sequence [In,As,In,As, substrate] with 2 ML of As (curve c). As in the (110) plane, almost all the bulk features are obtained with 3 ML of As (curve d) corresponding to the sequence [As,In,As,In,As, substrate]. However, the peak at 10° arises only when the slab contains the sequence [In,As,In,As,In,As,In,As, substrate] with 4 ML of As (curve g), namely, when As-In scatter-

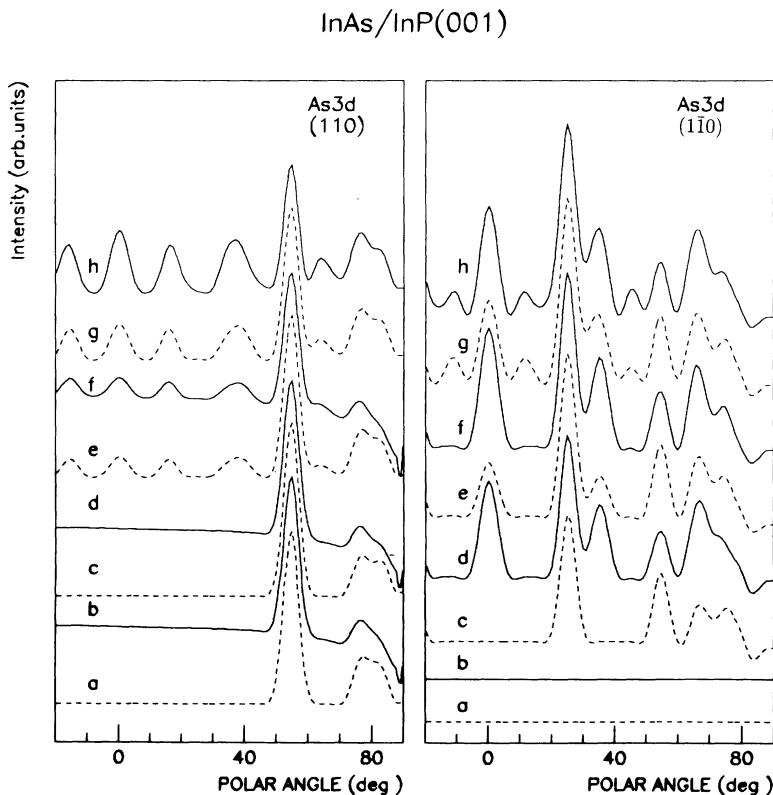


FIG. 7. Simulation of As 3d XPD curves corresponding to a layer-by-layer growth of InAs on an InP(001) sample. The dashed lines and the plain lines correspond to an In monolayer (1 ML) as the top layer and to an As monolayer (1 ML) as the top layer, respectively. The sequences are the following: (a) [In,As, substrate], i.e., one monolayer (1 ML) of As or one bilayer (1 BL) of InAs, (b) [As,In,As, substrate], i.e., 2ML of As or 2 BL of InAs, (c) [In,As,In,As, substrate], i.e., 2 ML of As or 2 BL of InAs, (d) [As,In,As,In,As, substrate], i.e., 3 ML of As or 3 BL of InAs, (e) [In,As,In,As,In,As, substrate], i.e., 3 ML of As or 3 BL of InAs, (f) [As,In,As,In,As,In,As, substrate], i.e., 4 ML of As or 4 BL of InAs, (g) [In,As,In,As,In,As,In,As, substrate], i.e., 4 ML of As or 4 BL of InAs, (h) [As,In,As,In,As,In,As,In,As, substrate], i.e., 5 ML of As or 5 BL of InAs.

ing events at 11° are allowed. This peak may be considered as the signature of the bulk property. The above-described curves may be used to quantify As penetration since the intensity collected by the detector is the sum of the intensities emerging from the chemically identical atoms: a simple addition of the above curves with the correct ratio can give the required estimation. Nevertheless, such an approach cannot be used to estimate the proportion of As atoms which are below the first four bilayers via the As-P substitution.

Figure 8 displays the experimental As 3*d* and In 3*d* PAD's for the (110) plane for As-stabilized InP surfaces heated at three typical temperatures: 450°C corresponding to a 1.25-As-equivalent monolayer, 550°C corresponding to a 1.65-As-equivalent monolayer, and 575°C corresponding to a 2.6-As-equivalent monolayer. These values were obtained by precise XPS measurements.²⁴ We also know from the observed RHEED patterns that we have in the top layer 1 ML of As at 450°C, 0.25 ML of As at 570°C, and in between at 550°C. This means that 0.25 ML of As at 450°C and 2.35 ML of As at 570°C are available for the layers below the top layer. Let us now focus on the As 3*d* emission, the In 3*d* PAD's being taken as references for the polar angles. The peak around 55° in the As 3*d* curve at 450°C unambiguously confirms that some As atoms are present in the third layer from the top and indicates the formation of InAs (curve b of Fig. 7). The As 3*d* curve at 550°C exhibits weak XPD peaks at 0° , 16° , and 35° due to some As atoms farther down in the bulk (curve f of Fig. 7). These three peaks become stronger when the sample is heated at 575°C under As pressure. Such a direct comparison of these experimental data with the curves of Fig. 7 clearly shows that the structure of an As-stabilized InP(001) surface

can be better described by a multilayer InAs/InAs_xP_(1-x)/InP model than by a layer-by-layer InAs/InP model. All the XPD peaks appear in the experimental curves even though there are less than 2.6 ML of As at 550°C and there are 2.6 ML of As at 575°C, instead of the 3 ML needed in the layer-by-layer model (Fig. 7). Figure 8 shows three calculated curves which correspond to a combination of curves (b) and (f) (chosen because they correspond to As-rich surfaces) with the ratios (100%,0%), (35%,65%), and (5%,95%), respectively. These ratios have been adjusted to reproduce the relative XPD peak intensities in the curves at 450°C, 550°C, and 575°C. We can see that the depth distribution becomes more and more uniform as the temperature increases [closer to curve (f) than to curve (b)] within the first four bilayers. However, from As 3*d* PAD's, it is impossible to decide whether or not the As atoms penetrate farther in the crystal than the sixth layer beyond the surface, since from the XPD point of view convergence is completely reached in curve f of Fig. 7. Finally, in Fig. 8, we note the broadness of the peak around 55° in the As 3*d* PAD's at 450°C and the unusual intensity of the shoulder at higher angle. The shape of this structure (not predicted theoretically) may be due to As atoms shifting slightly from their ideal lattice positions. This assumption is based on the fact that this broadening gradually disappears when the temperature increases. At the same time, the RHEED pattern changes from the (2×1) As-rich structure (450°C) to the (4×2) In-rich structure (570°C) with an intermediate step without twofold periodicity (550°C). Looking now to the backgrounds, we see that the slowly varying part of the As 3*d* PAD's evolve as expected in view of the extreme surface distribution of As. For In 4*d* PAD's, it remains close to that of the InP bulk

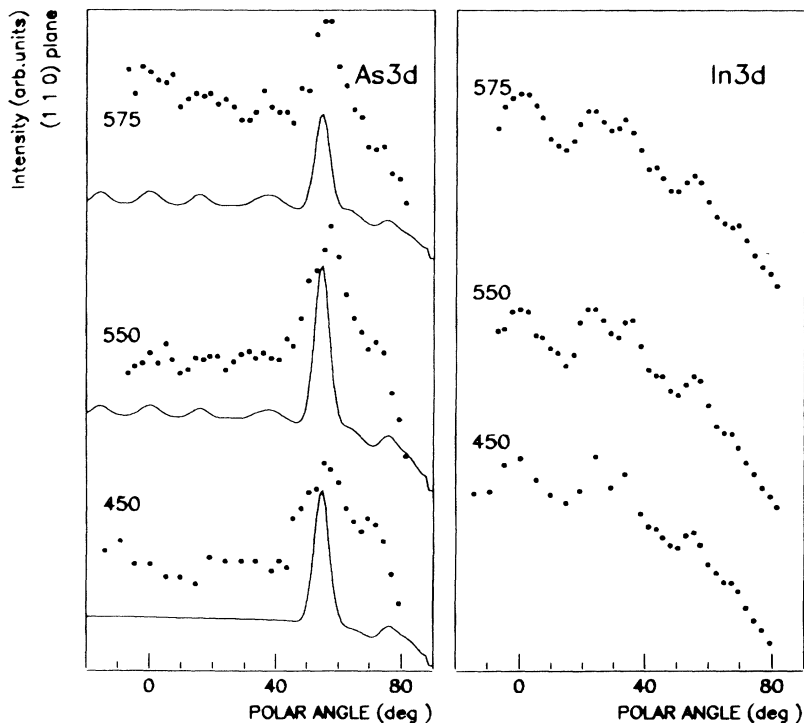


FIG. 8. Experimental polar plots for the As 3*d* and the In 3*d* core levels in the (110) plane for three As-stabilized InP(001) surfaces prepared with annealing temperatures equal to 450°C, 550°C, and 575°C. The calculated curves (indicated by plane lines) correspond to combining curves b and f of Fig. 7 in the ratios (100%,0%), (35%,65%), and (5%,95%), respectively.

sample (Fig. 5) even though 5 Å of InAs have been grown.

D. Investigation of the strain effects at the InAs/InP interface

When the heterojunction like InAs/InP is formed between two lattice-mismatched semiconductors, first, a thin ideal pseudomorphic InAs layer is expected to grow, and then the high strain energy stored in the InAs layer induces the formation of 3D islands and misfit dislocations. In the InAs/InP case, the onset of 3D growth occurs at about 8–10 Å for growth performed at 450°C and plastic relaxation begins at 20 Å.^{12,13} Very few experimental techniques allow measurement of the vertical strain (a_{\perp}) in such thin films as does XPD. As a matter of fact, GIXRD and RHEED can only provide a direct measurement of the in-plane strain distribution (a_{\parallel}).

In Figs. 9 and 10, we show the PAD's within the ($\bar{1}\bar{1}0$) plane and within the (110) plane, respectively, for two InAs films obtained by MBE growth on an As-stabilized InP substrate: (i) a strained 10-Å-thick InAs film and (ii) a partially (50%) relaxed 36-Å-thick InAs film, in addition to the PAD's for the above-studied bulk InAs samples used as references. The corresponding PAD's appear similar to those of bulk InAs except that the diffraction peaks at grazing angles (55° and especially 65°) exhibit a higher intensity. This observation can be related to the surface morphology of the InAs films. As already mentioned (Fig. 1), the surfaces of the 10- and 36-Å InAs films display 3D islands (elongated in the [$\bar{1}\bar{1}0$] direction with facets corresponding to (114) planes), favoring the elastic relaxation of the surface top layers.

Indeed, this roughness leads to an increasing number of atoms in a surface position and thus to an increasing number of broken bonds used as degrees of freedom to dissipate part of the strain energy. In contrast to the (110) planes which exhibit almost the same geometry as in Fig. 2, the ($\bar{1}\bar{1}0$) planes now show jagged lines since they are perpendicular to the island elongation direction, as may be seen in Fig. 11. With such a geometry, it is obvious that the number of diffraction events at the grazing angle is proportionally higher than for flat surfaces, in accordance with the experimental observation. The same explanation can be used to understand why the backgrounds of the As 3*d* PAD's increase from the normal to the grazing angles for the 10-Å InAs film (and to a lesser extent for the 36-Å InAs film) even more than for the few InAs layers shown in Fig. 8. We believe that the shape of such backgrounds could be a clear indication of the flatness of the surface: rough surfaces lead to higher intensities at grazing angles than flat surfaces. From the XPD point of view, this organized surface roughness induces real dissymmetry between the PAD's within the ($\bar{1}\bar{1}0$) plane and those within the (110) plane: the effects from the strain are more detectable and thus easier to quantify within the ($\bar{1}\bar{1}0$) plane As 3*d* PAD's than within the (110) plane As 3*d* PAD's.

Let us now focus on quantification of the strain using the diffraction peak at 55° in the As 3*d* PAD's within this ($\bar{1}\bar{1}0$) plane. The PAD for the strained 10-Å InAs film clearly shows a sizable contraction of the XPD structures toward the sample normal with a shift of 3° for the 55° peak. For the partially relaxed 36-Å InAs film, the XPD features are a superposition of peaks corresponding to re-

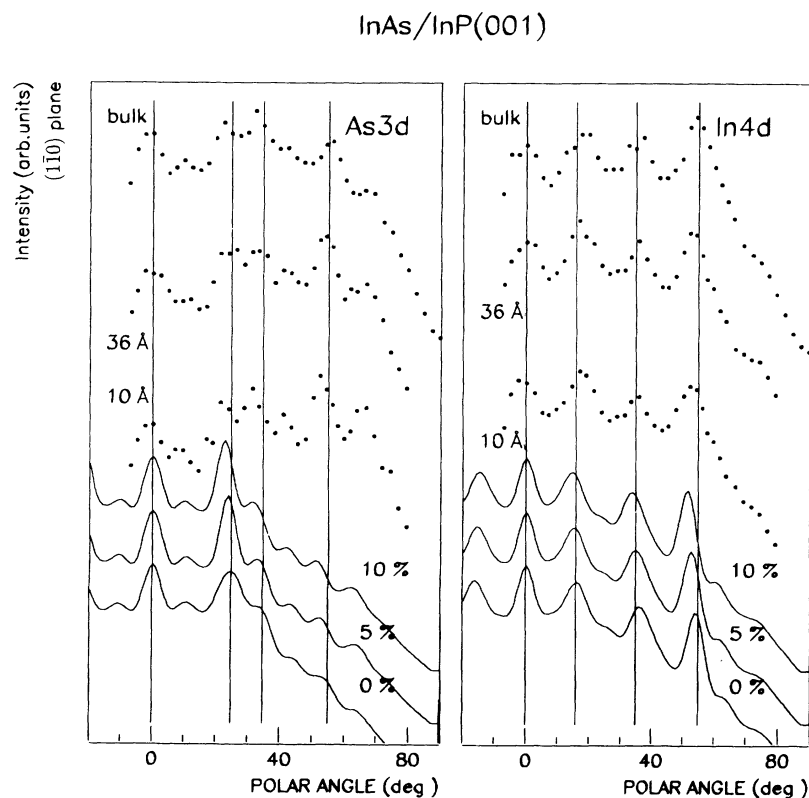


FIG. 9. Experimental polar plots for the As 3*d* and the In 4*d* core levels in the ($\bar{1}\bar{1}0$) plane for strained (10 Å) and partially relaxed (36 Å) InAs films grown on InP(001). Calculations (indicated by plain lines) are without any surface reconstruction and correspond to 0%, 5%, and 10% expansion in the [001] direction.

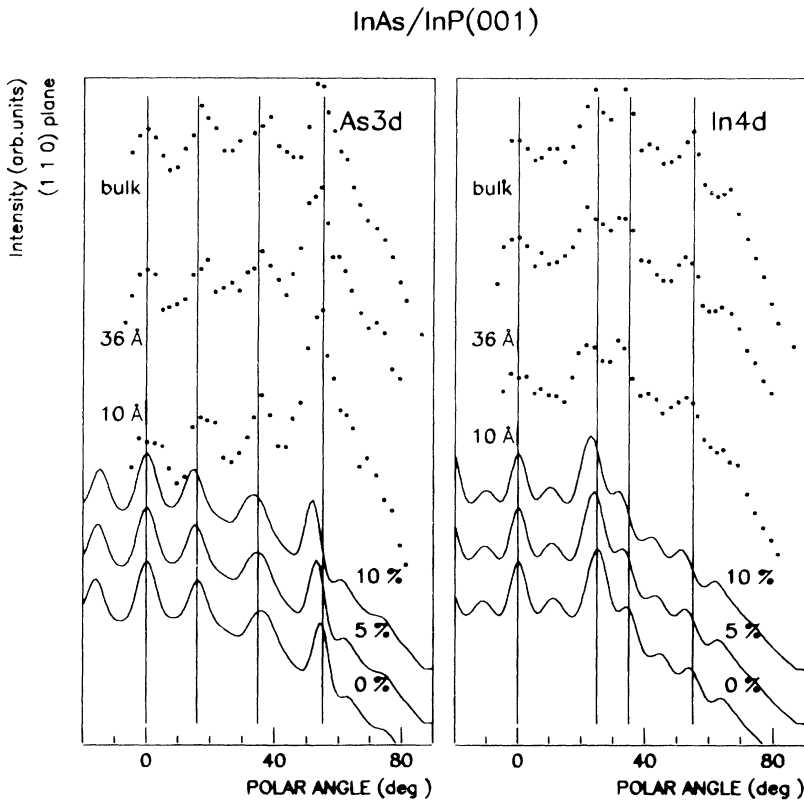


FIG. 10. Experimental polar plots for the As 3d and the In 4d core levels in the (110) plane for strained (10 Å) and partially relaxed (36 Å) InAs films grown on InP(001). Calculations (indicated by plain lines) are without any surface reconstruction and correspond to 0%, 5%, and 10% expansion in the [001] direction.

laxed and unrelaxed atomic positions. This results in the broadening of the As 3d XPD features observed for the 36-Å InAs film within the (110) plane. These experimental curves are compared in Figs. 9 and 10 with theoretical polar curves for InAs layers having a vertical lattice expansion of 5% and 10%. The calculations were performed with the scattering amplitudes relevant to InAs but taking the InP lattice constant $a = 5.8684 \text{ \AA}$ as a_{\parallel} and increasing this InP lattice constant in the [001] direction by 5%, i.e., $a_{\perp} = 6.1618 \text{ \AA}$, and by 10%, i.e., $a_{\perp} = 6.4552 \text{ \AA}$. Comparison of the 10-Å experimental and calculated curves shows that the best agreement is estimated to be around $(7.5 \pm 0.5)\%$ and thus corresponds to an a_{\perp} of 6.3085 \AA . Let us discuss more quantitatively the absolute value of this shift using two possible structural models.

A first way to model the structural properties of the interface may be to assume an atomically abrupt InAs/InP interface. The InAs film matches the InP lattice in the direction parallel to the interface (a_{\parallel}) and expands in the perpendicular direction (a_{\perp}). The magnitude of this vertical expansion may be estimated using macroscopic linear elasticity theory using the following relation,²⁵

$$a_{\perp} = a_0 + 2C_{12}/C_{11}(a_0 - a_{\parallel}),$$

where a_0 , a_{\perp} , and a_{\parallel} are the relaxed, the perpendicular, and the in-plane lattice parameters of the tetragonal structure, respectively, and where C_{11} and C_{12} are the elastic constants. For the particular case of strained InAs on InP, we have a_{\parallel} equal to $a_{\text{InP}} = 5.869 \text{ \AA}$, a_0 equal $a_{\text{InAs}} = 6.058 \text{ \AA}$, $C_{11} = 11.9 \times 10^{11} \text{ dyn/cm}^2$, and

3D islands

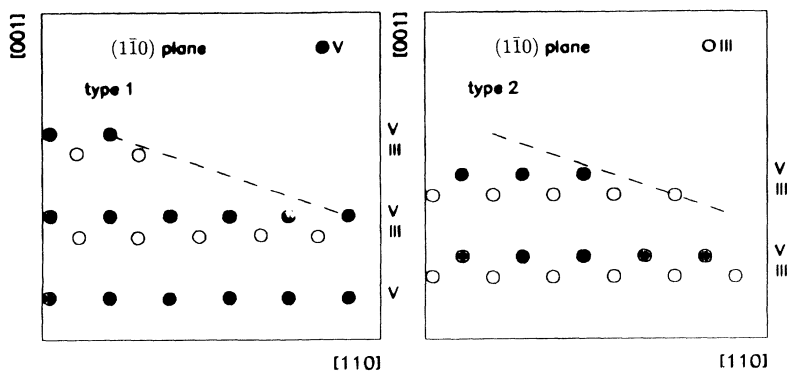


FIG. 11. Projections of the 3D islands on the low-index plane (110). The broken lines indicate the position of the (114) faceting within the two types of planes.

$C_{12} = 5.38 \times 10^{11} \text{ dyn/cm}^2$,²⁵ and thus we find $a_{\perp} = 6.229 \text{ \AA}$, which means an expansion of $\sim 6.1\%$ of a_{\perp} when compared to a_{\parallel} . This implies that peak d (Fig. 3) must have shifted from 55.7° to 53.1° . Such a result cannot be directly applied in our case, since it is now well known that the macroscopic continuum elasticity theory fails for the description of very thin films and interfaces. The top surface layer is generally not subjected to the same elastic constraints as bulk layers.

The second approach to predicting local atomic configurations in very thin films and interfaces is to assume the conservation of chemical bond lengths. As an example, if we assume that the In-As bond length keeps its bulk value (2.624 \AA) a 9.5% vertical expansion would be expected and peak d (Fig. 3) should shift from 55.7° to 52.3° . The vertical expansion of 7.5% from the XPD measurements thus falls between the 6.1% value from macroscopic linear elasticity theory and the 9.5% from conservation of the atomic bond length.

IV. CONCLUDING REMARKS

We have applied the XPD technique to characterize (i) the growth of InAs/InP(001) heterostructures by As stabilization of InP(001) surfaces, and (ii) the strain at the InAs/InP interfaces. In order to separate the different parameters which can affect the positions and intensities of XPD peaks, we have compared experimental results for the thin films with those for (i) a bulk InAs(001) sample, (ii) a bulk InP(001) sample, and (iii) a (2×4) recon-

structed GaAs(001) sample. It appears that almost all the XPD peaks may be directly associated with internuclear directions, due to the strong forward scattering occurring for photoelectrons having a high kinetic energy, interferences playing a rather minor role in this particular case. The observed features can therefore be directly interpreted in terms of geometric structure. Throughout this work, we have compared the experimental data with SSC calculations. We have shown via the study of the (2×4) reconstructed GaAs(001) sample how to minimize the overlapping of effects from bulk with those from the surface reconstruction effects, by using PAD's within the (110) and $(\bar{1}\bar{1}0)$ planes. The effects of the dissymmetric surface roughness due to 3D islands, of the As-P exchange as a growth mode, and of the strain have been qualitatively and semiquantitatively estimated from XPD patterns. The main difficulty lies in separating the particular contribution of each effect. In conclusion, it appears that XPD at grazing angles can be sensitive to the average surface roughness and thus could be used to qualify the flatness of a substrate or of an epitaxial layer. In addition, its unique ability of measuring the a_{\perp} parameter in very thin highly strained layers can be used to study the elastic relaxation of 3D islands via a comparison with the corresponding 2D-grown layers. This implies great experimental accuracy in the diffraction-angle measurements.

ACKNOWLEDGMENTS

LEAME is a Unité associée au CNRS 848.

¹S. A. Chambers, *Adv. Phys.* **40**, 357 (1991).

²S. A. Chambers, *Surf. Sci. Lett.* **248**, L274 (1991).

³P. Alnot, J. Olivier, F. Wyczisk, and C. S. Fadley, *J. Electron. Spectrosc. Relat. Phenom.* **43**, 263 (1987).

⁴S. A. Chambers and V. A. Loeb, *Phys. Rev. B* **42**, 5109 (1990).

⁵S. A. Chambers and V. S. Sundaram, *Appl. Phys. Lett.* **57**, 2342 (1990).

⁶S. A. Chambers, S. B. Anderson, H. W. Chen, and J. H. Weaver, *Phys. Rev. B* **34**, 913 (1986).

⁷R. Baptist, S. Ferrer, G. Grenet, and H. C. Poon, *Phys. Rev. Lett.* **64**, 311 (1990).

⁸G. S. Herman, A. P. Kaduwela, D. J. Friedman, M. Yamada, E. L. Bullock, C. S. Fadley, Th. Lindner, D. Ricken, A. W. Robinson, and A. M. Bradshaw, in *The Structure of Surfaces III*, edited by S. Y. Tong, M. A. Tong, M. A. Van Hove, K. Takayanagi, and X. D. Xie, Springer Series in Surface Sciences Vol. 24 (Springer-Verlag, Berlin, 1991).

⁹S. A. Chambers, *Phys. Rev. B* **42**, 10 865 (1990).

¹⁰C. S. Fadley, in *Synchrotron Radiation Research: Advances in Surface Science*, edited by R. Z. Bachrach (Plenum, New York, 1990).

¹¹W. F. Egelhoff, Jr., *Crit. Rev. Solid State Mater. Sci.* **16**, 213 (1990).

¹²G. Hollinger, M. Gendry, J. L. Duvault, C. Santinelli, P. Ferret, C. Miossi, and M. Pitaval, *Appl. Surf. Sci.* **56-58**, 665 (1991).

¹³G. Hollinger, D. Gallet, M. Gendry, C. Santinelli, and P. Vik-

torovitch, *J. Vac. Sci. Technol. B* **8**, 832 (1990).

¹⁴G. J. Whaley and P. I. Cohen, in *Layered Structures: Heteroepitaxy, Superlattices, Strain, and Metastability*, edited H. Pollak, MRS Symposia Proceedings No. 160 (Materials Research Society, Pittsburgh, 1990), p. 35.

¹⁵V. Swaminathan, in *Indium Phosphide and Related Materials: Processing, Technology and Devices*, edited by A. Katz (Artech House, Boston, 1992).

¹⁶M. Fink and A. C. Yates, *At. Data* **1**, 385 (1970); M. Fink and J. Ingram, *ibid.* **4**, 129 (1972); D. Gregory and M. Fink, *ibid.* **14**, 39 (1974).

¹⁷J. Muste de Leon, J. J. Rehr, C. R. Natoli, C. S. Fadley, and J. Osterwalter, *Phys. Rev. B* **39**, 5632 (1989).

¹⁸I. Tanaka, S. Ohkouchi, T. Kato, and F. Osaka, *J. Vac. Sci. Technol. B* **9**, 2277 (1991).

¹⁹M. D. Pashley, K. W. Haberern, W. Friday, J. M. Woodall, and P. D. Kirchner, *Phys. Rev. Lett.* **60**, 2176 (1988).

²⁰P. K. Larsen and D. J. Chadi, *Phys. Rev. B* **37**, 8282 (1988).

²¹G. X. Qian, R. M. Martin, and D. J. Chadi, *Phys. Rev. B* **38**, 7649 (1988).

²²M. D. Pashley, *Phys. Rev. B* **40**, 10 481 (1989).

²³D. K. Biegelsen, R. D. Bringans, J. E. Northrup, and L. E. Swartz, *Phys. Rev. B* **41**, 5701 (1990).

²⁴D. Gallet, M. Gendry, G. Hollinger, A. Overs, G. Jacob, B. Boudart, M. Gauneau, H. L'Haridon, and D. Lecrosnier, *J. Electron. Mater.* **20**, 963 (1991).

²⁵J. Hornstra and W. J. Bartels, *J. Cryst. Growth* **14**, 518 (1978).

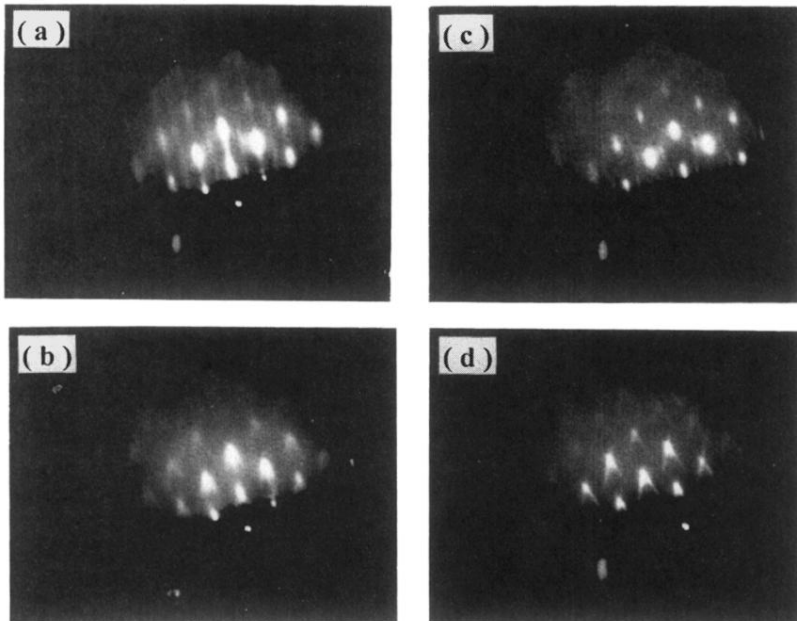


FIG. 1. RHEED patterns for (a) a 10-Å-thick InAs film grown on InP(001) along the [110] direction, (b) a 10-Å-thick InAs film grown on InP(001) along the $[1\bar{1}0]$ direction, (c) a 36-Å-thick InAs film grown on InP(001) along the [110] direction, and (d) a 36-Å-thick InAs film grown on InP(001) along the $[1\bar{1}0]$ direction. The V-shaped spots indicate a (114) faceting.

Unreconstructed III–V semiconductor

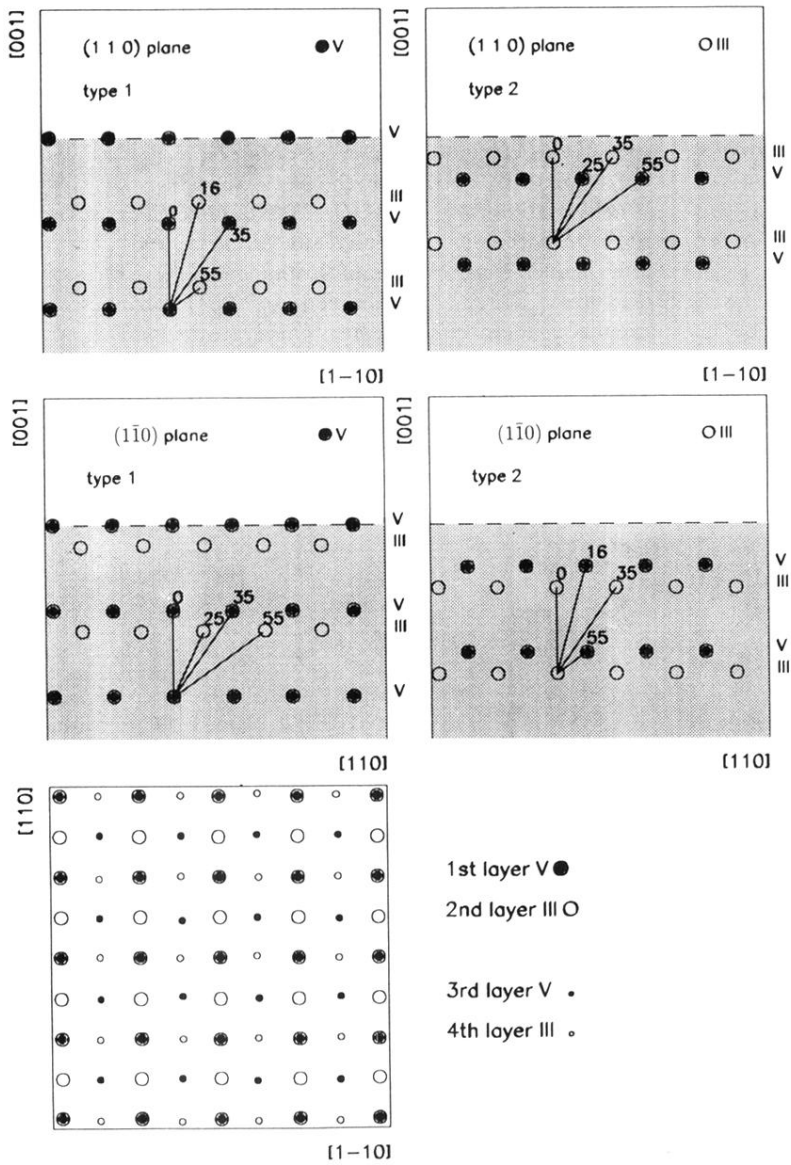


FIG. 2. Projections of the zinc-blende structure on the low-index planes (001), (110), and $(\bar{1}\bar{1}0)$. The main internuclear axes are indicated for the group-III element and the group-V element as emitters.